Acta Neuropathologica Communications

RESEARCH

Open Access

Hippocampal mitophagy alterations in *MAPT*-associated frontotemporal dementia with parkinsonism

Tyrique Richardson[1†], Xu Hou[1*†], Fabienne C. Fiesel[1,2], Zbigniew K. Wszolek[3], Dennis W. Dickson[1,2] and Wolfdieter Springer[1,2*]

Abstract

The enzyme pair PINK1 and PRKN together orchestrates a cytoprotective mitophagy pathway that selectively tags damaged mitochondria with phospho-serine 65 ubiquitin (pS65-Ub) and directs them for autophagic-lysosomal degradation (mitophagy). We previously demonstrated a significant accumulation of pS65-Ub signals in autopsy brains of sporadic Lewy body disease and Alzheimer's disease cases, which strongly correlated with early tau pathology. In this study, we extended our analysis to a series of pathologically confirmed cases of frontotemporal dementia with parkinsonism linked to chromosome 17 (FTDP-17) harboring different pathogenic mutations in *MAPT*, the gene encoding tau. We assessed the morphology, levels, and distribution of the mitophagy tag pS65-Ub in several affected brain regions and hippocampal subregions of these cases. While tau pathological burden was similarly increased across all FTDP-17 cases, pS65-Ub immunopositive signals were strongly accumulated in P301L cases and only weakly present in N279K cases. In the hippocampus of both mutation groups, the density of pS65-Ub positive cells was overall the greatest in the dentate gyrus followed by the subiculum, CA1, and CA2/3, with the CA4 showing only minimal presence. Notably, positive cells in the subiculum carried greater numbers and particularly vacuolar pS65-Ub structures, while cells in the dentate gyrus mostly contained fewer and rather granular pS65-Ub inclusions. Single cell analyses revealed differential co-localization of pS65-Ub with mitochondria, autophagosomes, and lysosomes in these two regions. Together, our study demonstrates distinct mitophagy alteration in different FTDP-17 *MAPT* cases and hint at selective organelle failure in the hippocampal subregions that was associated with the P301L mutation.

Keywords Frontotemporal dementia with parkinsonism, Hippocampus, *MAPT* P301L, Mitochondria, Mitophagy, Parkin, Phosphorylated ubiquitin, PINK1, PRKN, Tau

†Tyrique Richardson and Xu Hou contributed equally to this work.

*Correspondence:
Xu Hou
Hou.Xu@mayo.edu
Wolfdieter Springer
Springer.Wolfdieter@mayo.edu
[1]Department of Neuroscience, Mayo Clinic, Jacksonville, FL, USA
[2]Neuroscience PhD Program, Mayo Graduate School of Biomedical Sciences, Mayo Clinic, Jacksonville, FL, USA
[3]Department of Neurology, Mayo Clinic, Jacksonville, FL, USA

Introduction

Frontotemporal dementia with parkinsonism linked to chromosome 17 (FTDP-17) is a rare autosomal dominantly inherited neurodegenerative disorder [8, 16, 24, 25, 51, 60, 61], often associated with mutations in the microtubule-associated protein tau gene (*MAPT*) [3, 20]. While the clinical presentation varies, common features include parkinsonism, cognitive impairment, language difficulties, and other changes in personality, social behavior, and emotional regulation [60, 61]. Pathologically, varying degrees of atrophy have been observed in the frontal and temporal lobes, hippocampus, and basal ganglia as well as relatively wide-spread neuronal loss and gliosis within specific regions [2, 44, 58]. Two of the most frequent *MAPT* variants in FTDP-17 are N279K and P301L [20, 44] that both locate to exon 10 and specifically affect 4-repeat (4R) tau isoform [8, 22, 43]. The N279K mutation was reported to result in more frequent incorporation of exon 10 into transcripts and increase the production of 4R tau [13, 59]. Although P301L mutant tau seems to have limited ability to initiate aggregation, enhanced seeding capacity and contribution to the spread of pathologic tau between cells was shown (as reviewed in [49]). Despite the different mechanisms, both variants contribute to the formation of abnormal tau aggregates in neurons and glia, a hallmark pathology of FTDP-17 [25, 48, 55].

Mitophagy is a cytoprotective mitochondrial quality control mechanism for the timely elimination of damaged or dysfunctional mitochondria to maintain cellular homeostasis [54]. One of the best characterized mitophagy pathways is directed by the ubiquitin (Ub) kinase PINK1 and the Ub ligase Parkin/PRKN. Together they selectively decorate damaged mitochondria with phospho-serine 65 ubiquitin (pS65-Ub) [19, 54]. As a result of this specific labeling, damaged mitochondria are recognized by autophagic receptors and then directed for lysosomal degradation. Under stress or disease conditions, the accumulation of pS65-Ub may occur through increased mitochondrial dysfunction or impaired autophagic-lysosomal flux [19, 26, 54]. In human autopsy brain, we have previously documented the deposition of pS65-Ub into either granular or vacuolar structures during normal aging as well as in neurodegenerative conditions including Lewy body disease (LBD) and Alzheimer's disease (AD) [26–28]. The diverse morphology and co-localization profiles of pS65-Ub positive structures suggested distinct mitochondrial or lysosomal impairments in different brain regions that may contribute to the selective vulnerability in neurodegenerative diseases [27].

The accumulation of the mitophagy tag pS65-Ub was strongly and independently associated with early tau pathology, particularly the pretangles in LBD and AD brains [41, 42, 54]. Given that tau aggregation is a hallmark pathology in *MAPT*-associated FTDP-17, mitophagy alterations may also be present and contribute to the pathogenesis of this disease. We have previously observed abundant pS65-Ub inclusions in brains of old rTg4510 mice expressing human *MAPT* P301L mutation [27]. To investigate the impact of pathogenic *MAPT* mutations on mitophagy, we here measured pS65-Ub levels and distributions in several affected brain regions of a series of post-mortem FTDP-17 brains carrying either *MAPT* N279K or P301L mutations [8, 25, 51, 60]. In the hippocampal subregions, we further analyzed the morphology of pS65-Ub positive structures and their co-localization with different organelles involved in the mitophagy process (Fig. 1). Our study reveals significant hippocampal mitophagy alterations particularly in FTDP-17 with *MAPT* P301L mutation that may result from distinct organellar impairments within different hippocampal subregions.

Materials and methods

Human autopsy brains

A total of 20 autopsy brains were retrieved from the Mayo Clinic Florida Brain Bank. The cohort included FTDP-17 cases with *MAPT* N279K ($n=8$) or P301L ($n=3$) mutation that have been previously reported for the genetic, clinical, and neuropathological findings [8, 25, 51, 60] and age-matched neuropathologically normal controls ($n=9$). All *MAPT* N279K patients were from the same kindred, pallido-ponto-nigral degeneration family [60], while P301L patients were all from separate families [51]. All brains were examined and assessed in a standardized manner by a single neuropathologist. Available demographic and neuropathological information including age at death, sex, Braak tangle stage (0-VI), and Thal amyloid phase (0–5) are shown in Tables S1 and S2.

Immunohistochemical staining and image analysis

Immunohistochemical staining of paraffin-embedded post-mortem brain tissue was performed on sections containing various brain regions as previously described [27]. Sections were cut at 5 microns thickness and mounted onto slides to dry overnight at 60˚C. After deparaffinizing and rehydrating sections, antigen retrieval was performed by 30-minute steaming in deionized water. Immunohistochemistry was carried out using Envision Plus kit (Agilent, K4011, Agilent, K4007). Endogenous peroxidase blocking was performed for 5 min using 3% hydrogen peroxide (Swan, L0011380FB). Sections were blocked with 5% normal goat serum (Invitrogen, 16210-072) for 20 min and then incubated with primary antibodies against pS202-tau (CP13; monoclonal antibody from late Dr. Peter Davies, Feinstein Institute; 1:1000) or pS65-Ub (in-house [19, 26], 1:650) in Dako Antibody Diluent (Agilent, S3022) for 45 min at room temperature.

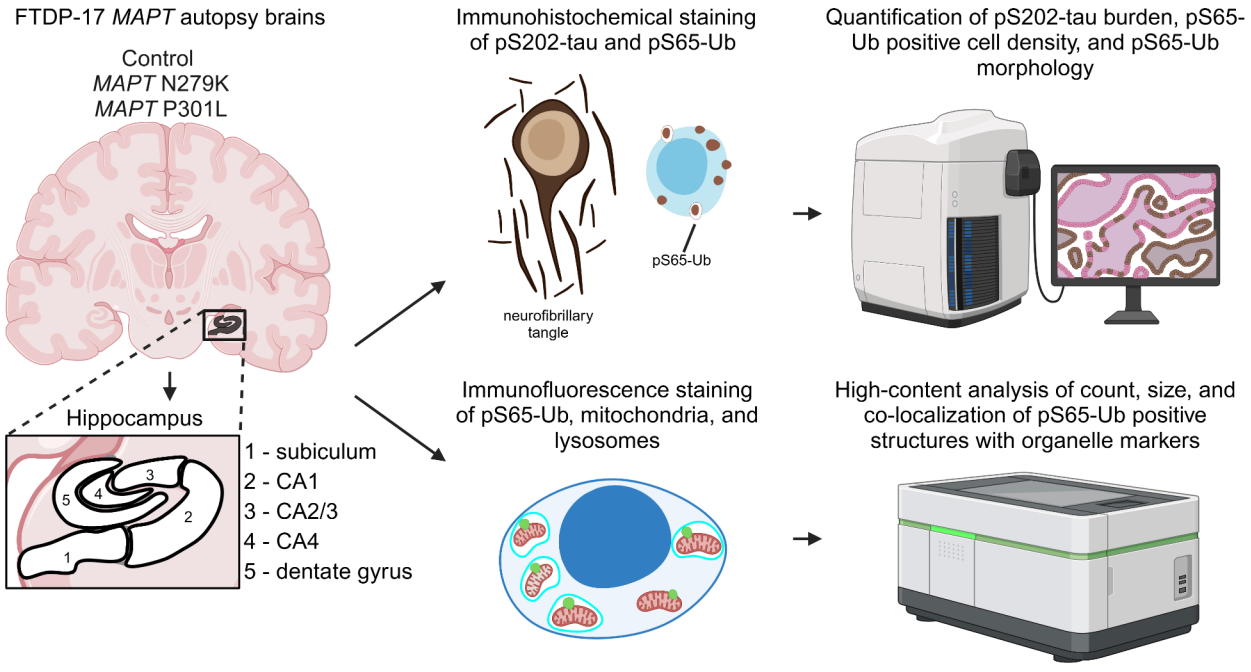

Fig. 1 Experimental workflow for cohort selection and imaging analysis of control and FTDP-17 *MAPT* mutant brains. A total of 11 FTDP-17 *MAPT* autopsy brains with either N279K or P301L mutations and 9 brains from age-matched controls were obtained from the brain bank. Sections containing hippocampi were immunohistochemically stained for mitophagy marker pS65-Ub and pS202-tau, and quantified for pS65-Ub cell density, pS202-tau burden, and tangle density within each hippocampal subregion (subiculum, CA1, CA2/3, CA4, dentate gyrus). Adjacent sections were also immunofluorescence stained for pS65-Ub, mitochondria, and lysosomes. The localization of pS65-Ub signals in different organelle compartments were quantified at single cell levels. Schematic created with BioRender.com

After sections were incubated with EnVision-Plus anti-rabbit or anti-mouse labeled polymer-HRP (Agilent, K4003; Agilent, K4007) for 30 min, peroxidase labeling was visualized with the DAB chromogen solution (Agilent, K3468). Counterstaining was performed with hematoxylin (Epredia, 6765006). Slides were coverslipped with Cytoseal XYL mounting media (Epredia, 8312-4) after dehydration. Stained sections were then scanned with an Aperio AT2 digital pathology scanner at 20x magnification (Leica Biosystems, Nussloch, Germany). The hippocampus, amygdala, nucleus basalis of Meynert, putamen, and five hippocampal subregions (subiculum, cornu ammonis [CA] 1, CA2/3, CA4, and dentate gyrus) were traced for image analysis in ImageScope (Version 12.4.2.7000).

Image analysis for pS202-tau burden was performed using an optimized positive pixel count algorithm that detected total positive pS202-tau structures (e.g. tangles and neuropil threads) (Fig.S1, middle column). Number of tau tangles were assessed using an optimized cell count algorithm (Fig. S1, right column). Tangle density was calculated by dividing the tangle count by the area of the corresponding brain regions. pS65-Ub positive cells were quantified manually. According to the number of pS65-Ub puncta each cell contained in the hippocampal subregions, pS65-Ub positive cells were categorized into low (≤ 4 puncta) and high (> 4 puncta) pS65-Ub groups. Based on the distinct morphology of pS65-Ub puncta, pS65-Ub positive cells were also categorized into primarily granular or vacuolar puncta-containing cells.

Immunofluorescence staining and high content imaging analysis

Immunofluorescence staining of paraffin-embedded post-mortem brain tissues was performed as previously described [27] in the hippocampal sections of three FTDP-17 *MAPT* P301L cases. Sections were cut at a thickness of 5 microns and mounted onto positively charged slides to dry overnight at 60˚C. After sections were deparaffinized and rehydrated, antigen retrieval was performed by 30-minute steaming in deionized water. Following 1 h blocking with the serum-free Protein Block (Dako, X0909), sections were incubated overnight at 4˚C with primary antibodies against pS65-Ub (in-house [19], 1:300), the mitochondrial marker SSBP1 (Santa Cruz Biotechnology, sc-34727, 1:50), the lysosomal marker

CTSD (MilliporeSigma, MA1013, 1:500), the autophagy marker p62/SQSTM1 (BD Biosciences, 610832, 1:250) or pS202-tau (CP13, 1:250) diluted in Dako Antibody Diluent (Dako, S3022). The next day sections were incubated with secondary antibodies (Invitrogen, A-21206, A-11057, and A-31571; 1:500) and DAPI (Sigma-Aldrich, D9542; 1:1000) at room temperature for 1.5 h, followed by 3 min incubation in Sudan Black (SPI Supplies, 02560-AB) and then coverslipped in fluorescence mounting medium (Dako, S3023). For triple staining of Thioflavin S, CP13, and pS65-Ub, slides were first incubated in aqueous Thioflavin S for 8 min at room temperature and then washed in 80% and then 95% ethanol as well as in distilled water before entering the target retrieval step. High-resolution confocal fluorescent images were taken with an AxioObserver microscope equipped with an ApoTome Imaging System (Zeiss, Oberkochen, Germany).

High content imaging and the quantification of pS65-Ub, SSBP1, and CTSD positive signals was performed with an Operetta CLS High Content imaging system (Perkin Elmer, Waltham, MA, USA) equipped with Harmony analysis software. Slides were initially imaged at 10x magnification to identify the subiculum and dentate gyrus regions. These two subregions were then imaged using a 63x water objective with z-stack consisting of 10 planes at a distance of 5 µm. Image analysis was performed using standard building blocks of the Harmony software (version 4.9). First, nuclei and cytoplasm were defined through 'find nuclei' based on DAPI staining and 'find cytoplasm' based on CTSD signal, respectively. pS65-Ub inclusions were identified through 'find spots' and pS65-Ub positive cells were separated based on the 'select population'. The signal intensity, area, and number of pS65-Ub inclusions per cell were then calculated. Approximately 30 pS65-Ub positive cells from the subiculum and 60 cells from the dentate gyrus were randomly selected for co-localization analysis using 'finding image regions' to identify regions with pS65-Ub and mitochondrial or lysosomal markers. The area of overlapping regions was calculated using 'morphology' and 'position properties' building blocks.

Statistical analysis

Statistical analysis was performed through GraphPad Prism (Version 9.2.0.). For comparison of three groups, one-way ANOVA and unpaired t-test followed by adjustment with Bonferroni correction for three pair-wise comparisons were used. For comparison between *MAPT* mutations, unpaired t-test was performed. Additionally, all tests were corrected for five hippocampal subregions. Statistical significances were given as adjusted p-values.

Results

Distinct tangle distribution and morphology in the hippocampus of FTDP-17 *MAPT* cases

To evaluate tau pathology in *MAPT*-associated FTDP-17 cases, we performed a comprehensive immunohistochemical analysis of autopsy brains with an antibody against pS202-tau (CP13). Both *MAPT* N279K and P301L mutation carriers exhibited widespread deposition of tau tangles and neuropil threads across multiple brain regions, including the frontal and temporal cortex, basal forebrain, hippocampus, thalamus, basal ganglia, midbrain, pons, and medulla [51]. N279K mutant cases showed additional tau pathology in the motor cortex and cerebellar white matter, regions that were largely spared in P301L mutant cases. Notably, N279K mutation carriers also exhibited a greater abundance of glial tau inclusions in most affected brain regions compared to P301L cases. Based on these findings, we selected four regions including the hippocampus, amygdala, nucleus basalis of Meynert, and putamen that were consistently and severely affected for a quantitative analysis of pS202-tau burden and tau tangle density using unbiased algorithms (Fig.S1& S2). The quantification showed that all four regions exhibited similarly high levels of total pS202-tau deposition compared to controls (Fig. S2A). However, P301L mutant cases exhibited significantly greater tau tangle density in most regions compared to N279K mutant cases, with the hippocampus showing the most pronounced increase (Fig. S2B). Closer inspection of the hippocampus revealed abundant pS202-tau immunoreactive structures including tau tangles, neuropil threads, and occasional glial inclusions as well as notable regional differences across subfields in both mutation groups (Fig. 2A).

We next quantified pS202-tau burden and tau tangle density in hippocampal subregions including the subiculum, CA1, CA2/3, CA4, and dentate gyrus. This confirmed significantly increased tau pathology across all subregions in both *MAPT* mutation groups compared to controls (Fig. 2B-C). While total pS202-tau burden was elevated in N279K and P301L mutant cases (Fig. 2B), P301L mutation carriers showed significantly greater tangle density than N279K mutation carriers in most subregions, except for CA4 (Fig. 2C). Among the hippocampal subregions, total pS202-tau burden was slightly greater in the subiculum compared to other subregions, whereas tau tangle density was the greatest in the dentate gyrus, likely due to the densely packed granule cells here, followed by the subiculum, CA1, CA2/3, and was the lowest in the CA4 (Fig. 2D). Upon closer examination of the tangle morphology [41, 42, 51], we noted that N279K mutant cases primarily contained mature, intensely stained late-stage tangles, whereas P301L mutant cases

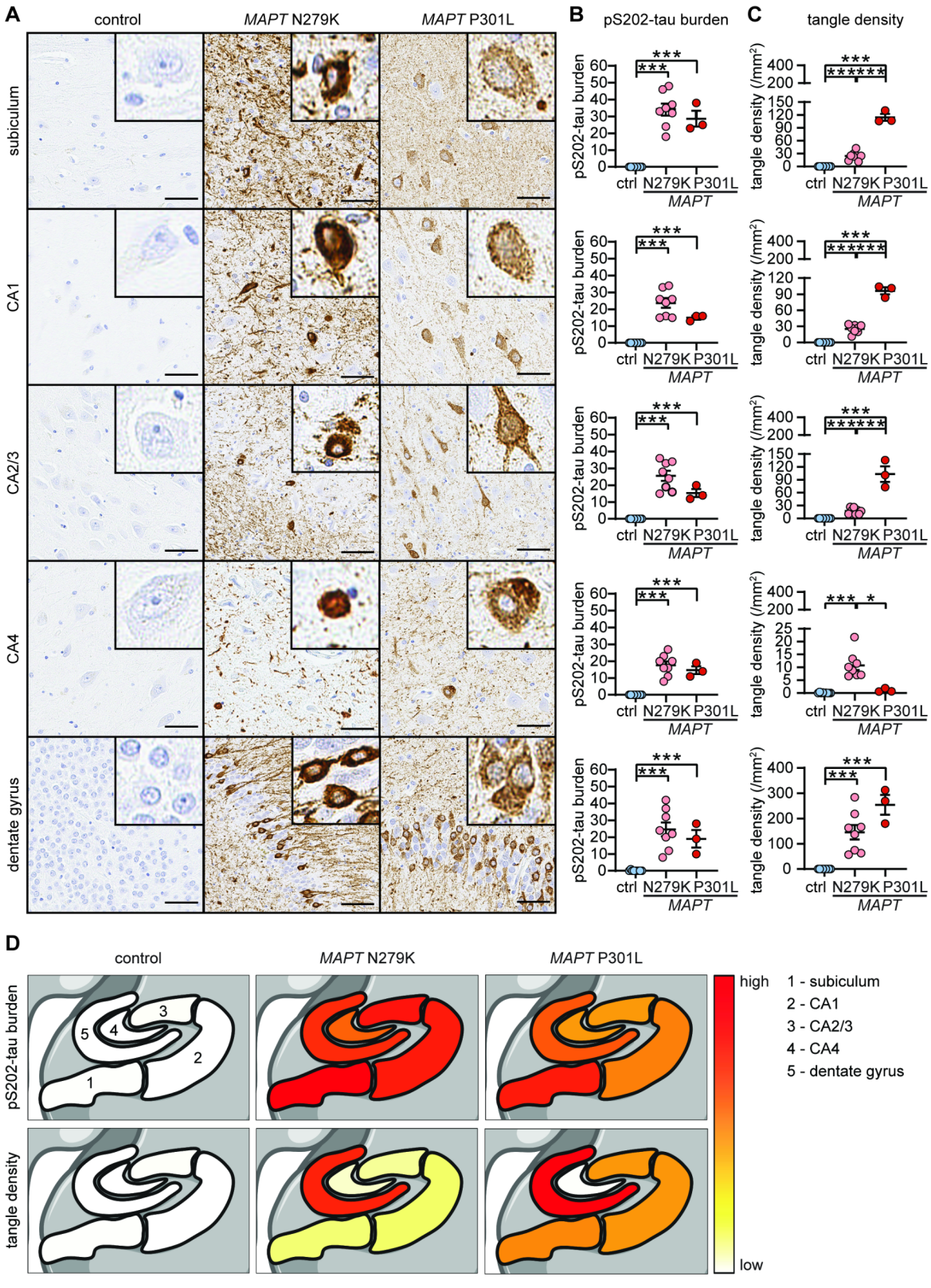

Fig. 2 (See legend on next page.)

(See figure on previous page.)

Fig. 2 Increased tau pathology but diverse tangle morphology in FTDP-17 *MAPT* mutant cases. (**A**) Representative images of hippocampal subregions from control and FTDP-17 *MAPT* cases stained with pS202-tau antibody CP13. Scale bars: 100 µm (**B**, **C**) Quantifications of total pS202-tau burden (**B**) and tau tangle density (**C**) in hippocampal subregions. Significantly higher levels of pS202-tau burden and tangle density were observed across most subregions in *MAPT* mutations cases compared to controls. P301L cases showed higher tangle density and pretangle tau pathology compared to the mature tangle pathology in N279K cases. (**D**) Heatmaps of pS202-tau burden and tangle density across hippocampal subregions in control and FTDP-17 *MAPT* mutation cases (1 = subiculum, 2 = CA1, 3 = CA2/3, 4 = CA4, 5 = dentate gyrus). Data are shown as mean ± SEM. Statistical analysis was performed using One-way ANOVA and then unpaired t-test followed by Bonferroni correction for multiple comparisons (*$p < 0.05$, **$p < 0.01$, ***$p < 0.001$). Controls: $n = 9$; N279K: $n = 8$; P301L: $n = 3$. Heatmaps created with BioRender.com

predominantly contained weakly stained pretangles by the pS202-tau antibody (Fig. 2A).

Cases with N279K mutation showed a notably greater abundance of intensely labeled neuropil threads, which were most prominent in the subiculum, followed by the CA1, CA2/3, and dentate gyrus, and the lowest in the CA4. In contrast, neuropil threads in the P301L mutant hippocampus were overall less immunoreactive, also being most abundant in the subiculum, but followed by the dentate gyrus and CA4, with the lowest levels in the CA1 and CA2/3 (Fig. 2A). Together, we demonstrated a comparable abundance of overall pS202-tau pathology in the hippocampus of FTDP-17 *MAPT* cases while observing distinct differences in morphology and subregional distribution of tau tangles and neuropil threads between N279K and P301L mutation carriers.

Altered mitophagy in select hippocampal subregions in FTDP-17 *MAPT* cases

To assess mitophagy alteration in the *MAPT*-associated FTDP-17 cases, sections of the hippocampus, amygdala, nucleus basalis of Meynert, and putamen from both mutation carriers and controls were stained for the mitophagy tag pS65-Ub (Fig. S2C). Amongst those regions, the greatest increase of pS65-Ub positive cell density was found in the hippocampus with notable regional differences between hippocampal subfields. Typical pS65-Ub immunopositive puncta were detected in hippocampal neurons across all subregions (Fig. 3A). Similar to the hippocampal tangle density, pS65-Ub positive cell density was substantially increased in most subregions of the P301L cases, except for CA4, when compared to controls and N279K cases (Fig. 3B). In certain subregions including the subiculum and CA2/3, a much smaller but significant increase in pS65-Ub was also observed in N279K mutant carriers compared to controls (Fig. 3B). Consistent with our previous finding [26, 27], pS65-Ub positive inclusions were frequently found in CP13 positive tau pretangles rather than in mature, Thioflavin S positive neurofibrillary tangles (Fig. S3). As greater tangle density may contribute to the additional pS65-Ub accumulation in P301L cases [26, 27], we adjusted pS65-Ub levels by tau tangle levels in both *MAPT* mutation groups. Even after normalization, pS65-Ub levels remained significantly higher in P301L compared to N279K carriers in the CA1, CA4, and dentate gyrus (Fig. 3C). When comparing all hippocampal subregions, pS65-Ub cell density was the highest in the dentate gyrus, again mainly due to the closely packed granule cells in this region, followed by the subiculum, CA1, and CA2/3 in the P301L cohort (Fig. 3D). Our results suggest a considerable mitophagy alteration in select hippocampal subregions of FTDP-17 *MAPT* cases particularly in those carrying the P301L mutation.

Distinct pS65-Ub puncta load and morphology in the hippocampal subregions of *MAPT* P301L mutant cases

The increased density of pS65-Ub positive cells in FTDP-17 *MAPT* disease cases reflected an overall alteration in mitophagy at the tissue level. However, this measure does not account for the abundance or morphology of pS65-Ub positive signals in individual cells. To further characterize mitophagy alterations in the hippocampal subregions of FTDP-17 *MAPT* mutant cases, we first categorized pS65-Ub positive cells into two groups with either low (≤ 4 counts) or high (> 4 counts) number of intracellular pS65-Ub puncta per cell (Fig. 4A). We observed significant increases in the density of both low- and high-puncta pS65-Ub positive cells in P301L compared to N279K mutation carriers across all subregions, except for CA4 (Fig. 4B). In P301L mutant brains, cells with low-count pS65-Ub puncta were primarily seen in the dentate gyrus, with more than 5-fold greater abundance over all other subregions. In contrast, cells with high-count pS65-Ub deposits were more frequently found in the subiculum, followed by the CA1 and CA2/3 regions (Fig. 4B). Based on the distinct morphologies of pS65-Ub inclusions, we next classified pS65-Ub positive cells into two groups that predominantly contain either granular or vacuolar puncta (Fig. 4C), which have been previously linked to more pronounced mitochondrial stress or reduced autophagic-lysosomal flux, respectively [27]. We again observed significant increases of both morphology groups in P301L compared to N279K mutation carriers across all hippocampal subregions, except for CA4 (Fig. 4D). pS65-Ub positive cells that contained primarily granular puncta were most frequently found in the dentate gyrus, while those carrying mainly vacuolar structures were most commonly found in the subiculum and CA1. Taken together, our results revealed a differential accumulation of pS65-Ub deposits with most prominent distinction of puncta load and morphology in the

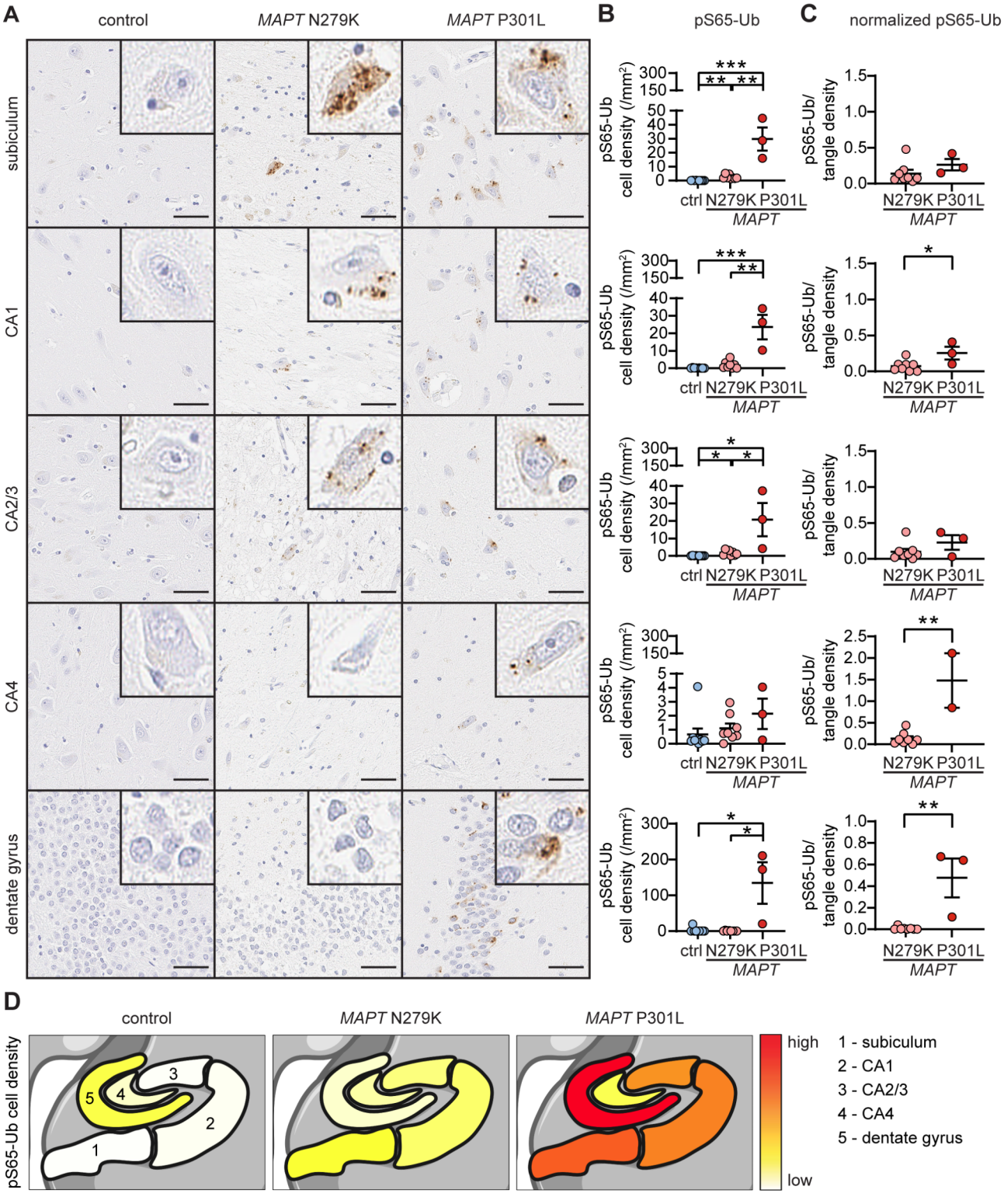

Fig. 3 (See legend on next page.)

(See figure on previous page.)

Fig. 3 Increased pS65-Ub levels in select hippocampal subregions in FTDP-17 *MAPT* mutant cases. (**A**) Representative images of hippocampal subregions from FTDP-17 *MAPT* and control cases stained with pS65-Ub. Scale bars: 100 µm (**B**) Quantification of pS65-Ub positive cell density in hippocampal subregions from FTDP-17 *MAPT* and control cases. Significantly increased pS65-Ub levels were observed in select hippocampal subregions of *MAPT* mutation carrier compared to controls. (**C**) Quantification of pS65-Ub positive cell density after adjustment for tangle density. P301L mutant cases retained significant higher levels of pS65-Ub compared to N279K mutation carrier in the CA1, CA4 and dentate gyrus after the normalization. (**D**) Heatmaps of pS65-Ub cell density across hippocampal subregions in control and FTDP-17 *MAPT* mutation cases (1 = subiculum, 2 = CA1, 3 = CA2/3, 4 = CA4, 5 = dentate gyrus). Data are shown as mean ± SEM. Statistical analysis was performed using One-way ANOVA and then unpaired t-test followed by Bonferroni correction for multiple comparisons (*$p < 0.05$, **$p < 0.01$, ***$p < 0.001$). Controls: $n = 9$; N279K: $n = 8$; P301L: $n = 3$. Heatmaps created with BioRender.com

subiculum and dentate gyrus of FTDP-17 brains with the *MAPT* P301L mutation.

Increased localization of pS65-Ub with lysosomes in the subiculum of *MAPT* P301L cases

Given that pS65-Ub positive cells were most abundant in the subiculum and dentate gyrus of the *MAPT* P301L mutant cohort, we next focused on these two subregions and performed detailed analysis at the single cell level. A first closer examination revealed a substantial difference in the pS65-Ub load per cell between these two regions. Although the dentate gyrus harbored the highest levels of pS65-Ub positive cells, the majority of these cells contained less pS65-Ub puncta and were categorized as low-count cells (Fig. 5A-B). Conversely, pS65-Ub positive cells in the subiculum showed a greater number of inclusions per cell, with many classified as the high-count category (Fig. 5A-B). Interestingly, pS65-Ub puncta in low-count cells were mostly granular in nature and were often found in the dentate gyrus. pS65-Ub puncta in high-count cells contained proportionally a larger number of vacuolar structures and were more often located in the subiculum (Fig. 5C-D).

To determine the intracellular compartment in which pS65-Ub accumulated, we examined co-localization of the mitophagy tag with mitochondrial (SSBP1) and lysosomal (CTSD) markers (Fig. 5E-F). In line with the immunohistochemical results, the high-resolution imaging confirmed significantly higher numbers of pS65-Ub inclusions per cell in the subiculum compared to the dentate gyrus (Fig. 5G). Although there was no difference in the average signal intensity of pS65-Ub puncta (Fig. 5G), pS65-Ub puncta in the subiculum were larger in size, consistent with their mostly vacuolar nature, as opposed to the mainly granular appearance in the dentate gyrus (Fig. 5G). Both mitochondria and lysosomes appeared more clustered in the subiculum, with some lysosomes forming intensely labeled, larger structures (Fig. 5E-F). In contrast, both organelles were more scattered throughout the cells in the granular neurons of the dentate gyrus. Quantification of both organelles showed that while the mitochondrial area per cell was comparable between the two subregions, there was a trend of increased lysosomal area per cell in the subiculum compared to the dentate gyrus (Fig. S4). Consistently, the percentage of co-localization of pS65-Ub inclusions with the mitochondrial marker was similar between the two subregions; however, co-localization with the lysosomal marker showed a trend towards an increase in the subiculum compared to the dentate gyrus (Fig. 5H-I). The results were statistically not significant likely due to the limited availability of the rare P301L mutation cases, yet align with the strong co-localization of pS65-Ub inclusions with the autophagy marker p62/SQSTM1 in the subiculum (Fig. S5).

Together, these findings highlight the distinct morphology of pS65-Ub positive puncta in cells from the subiculum and dentate gyrus and suggest that different organelle impairments may contribute to mitophagy alterations in two of the most affected hippocampal subregions.

Discussion

Mitochondrial dysfunction and the concomitant oxidative stress are hallmark features of the aging brain and are commonly observed also during the early stages of AD and other tauopathies, even before overt neurodegeneration occurs [6, 21]. Impaired mitophagy contributes to the accumulation of damaged mitochondria and therefore increases reactive oxygen species and metabolic stress. This may perpetuate a cycle of cellular toxicity to further promote tau aggregation [14], potentially playing a crucial role in disease pathogenesis. In previous work, we already identified a strong association between the accumulation of the mitophagy marker pS65-Ub and early tau pathology in autopsy brains from sporadic LBD and AD cases [26, 27]. Here, we expanded our investigation into a series of post-mortem FTDP-17 brains carrying either *MAPT* N279K or P301L mutations in which we determined pathological tau burden and tangle density, distribution and levels of the mitochondrial damage marker pS65-Ub, and morphologies of the deposits and their co-localization with different organelles involved in the mitophagy process.

The anatomical distribution of tau pathology in *MAPT*-associated FTDP-17 brains varies substantially depending on the specific tau mutations [20, 51]. The hippocampal region was strongly affected by tau pathology in both *MAPT* N279K and P301L mutation carriers. The tau tangle density was particularly high in the hippocampus of P301L cases compared to other affected regions such as the amygdala, nucleus basalis of Meynert, and putamen. Of note, there was marked heterogeneity in the tau

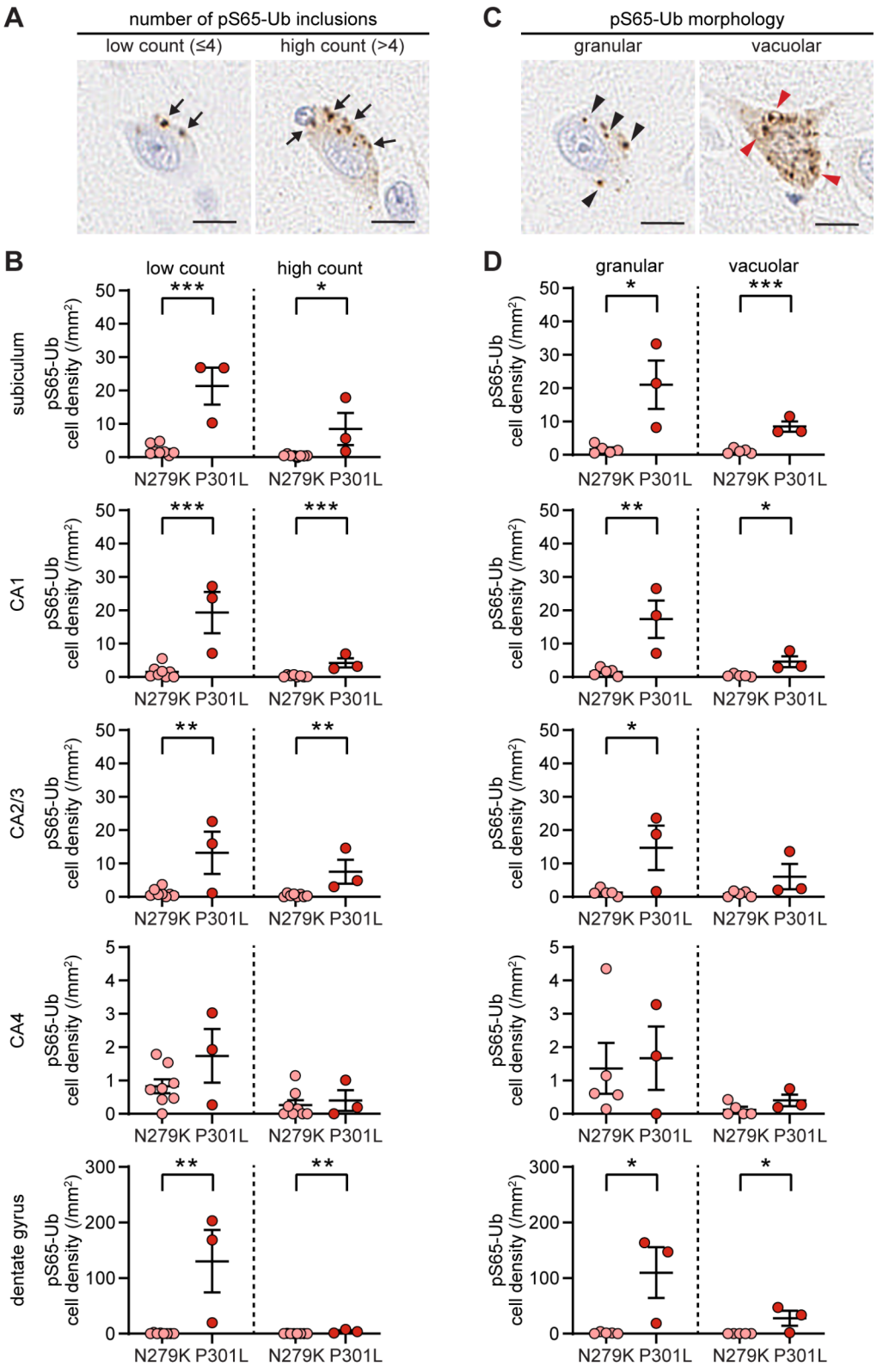

Fig. 4 (See legend on next page.)

(See figure on previous page.)

Fig. 4 Different load and morphology of pS65-Ub inclusions in hippocampal subregions of FTDP-17 *MAPT* mutant cases. (**A**) Representative images of low count (≤ 4 counts) and high count (> 4 counts) pS65-Ub inclusion-containing cells. Arrows pointing to individual pS65-Ub inclusion. Scale bars: 12.5 µm (**B**) Distribution of pS65-Ub positive cells into low- and high-count groups in five hippocampal subregions of FTDP-17 *MAPT* mutant cases. P301L mutant cases showed significantly higher levels of pS65-Ub in most groups and subregions except for CA4. N279K: $n = 8$; P301L: $n = 3$. (**C**) Representative images of pS65-Ub positive cells that primarily contained granular or vacuolar pS65-Ub inclusions. Black and red arrowheads pointing to individual granular and vacuolar pS65-Ub inclusions, respectively. Scale bars: 12.5 µm. (**D**) Quantification of granular and vacuolar pS65-Ub positive cells across five hippocampal subregions in FTDP-17 *MAPT* mutant cases. P301L cases showed significantly higher levels of granular and vacuolar morphology across most hippocampal subregions. Most granular and vacuolar cells were in the dentate gyrus, followed by the subiculum. N279K: $n = 5$; P301L: $n = 3$. Data are shown as mean ± SEM. Statistical analysis was performed using One-way ANOVA and then unpaired t-test followed by Bonferroni correction for multiple comparisons (*$p < 0.05$, **$p < 0.01$, ***$p < 0.001$)

pathology between mutation groups, likely due to diverse pathobiological effects of the respective mutant tau proteins [20]. Cases with N279K mutation exhibited more neuropil threads and predominantly mature, late-stage tangles, consistent with previous reports of an increased ratio of aggregation-prone 4R tau over 3R tau [13, 59] and the formation of generally larger filaments [20]. In contrast, P301L mutation carriers showed a more diffuse pattern with significantly greater number of pre-tangles, in agreement with another study [40] and overall smaller filaments formed by the mutation [20]. This may also reflect the limited ability of P301L tau to initiate aggregation, despite a significant seeding capacity and synaptic spread were shown in vitro and in vivo models [49].

While significant pathological tau burden was found in the hippocampi of both *MAPT* N279K and P301L mutation groups, pS65-Ub inclusions were markedly accumulated only in the P301L mutant brains. This increase remained in the CA4 and dentate gyrus even after normalizing for the greater tau tangle density in P301L mutant cases. The distribution of pS65-Ub positive cells in the hippocampal subregions closely mirrored the distribution of tau pretangles. These findings are consistent with our previous report in AD brains and transgenic mice overexpressing P301L tau, in which the pS65-Ub positive cell density was particularly high in the most affected regions and closely associated with early tau pathology, rather than with late-stage mature tangles [27]. The current study additionally demonstrated P301L mutant tau-associated alterations in PINK1-PRKN-directed mitophagy in *MAPT*-associated FTDP-17 brain. We and others have previously reported interactions between P301L mutant tau, PRKN, and altered mitophagy in neuroblastoma cells, *C. elegans*, and rTg4510 mice [9, 27]. However, these studies have yielded conflicting effects of P301L tau on the translocation of PRKN from the cytosol to mitochondria, with one showing enhanced translocation and the other indicating stalled movement. These discrepancies may be attributable to differences in the model organisms used as well as whether the targeted proteins were expressed at endogenous levels or overexpressed. The effect of N279K mutant tau on PINK1-PRKN signaling is however largely unexplored. Given that a significant shift of PRKN protein into the insoluble fraction was observed in AD brains [27, 62], it is possible that mature tau tangles in N279K cases sequester more PRKN protein, leading to depletion of this critical ubiquitin ligase from the soluble cytoplasmic pool, thereby affecting the production of pS65-Ub on the damaged mitochondria. Despite these variations, all studies consistently suggest that disease-associated tau impairs mitophagy [9, 17, 27, 29, 31, 32, 56], and PRKN overexpression was able to enhance the clearance of damaged mitochondria and reduce pathological burden [32].

Beyond the potential direct effects of P301L and N279K tau on PINK1-PRKN signaling, the accumulation of pS65-Ub may also result indirectly from increased mitochondrial damage or from impaired autophagic-lysosomal flux and clearance. Extensive literature has documented the impact of P301L tau on mitochondrial function, including alterations in mitochondrial morphology, content [33, 46], axonal transport [30], respiration, ATP synthesis [10, 12, 23, 45, 47], and mitochondrial dynamics [46, 47] in cell and transgenic mouse models. Recent proteomic studies revealed that mitochondrial proteins, such as various subunits of ATP synthase in complex V, were major tau interactors, and this interaction was significantly diminished in P301L tau- compared to wildtype tau-expressing neurons [15, 37, 53]. In contrast, while N279K tau was also shown to impair mitochondrial function in cultured neurons [34], the relatively preserved mitochondrial axonal transport, as compared to P301L tau neurons [59], may allow a more efficient mitochondrial turnover, resulting in reduced accumulation of pS65-Ub-labeled damaged mitochondria in the patient hippocampus. Furthermore, P301L tau has been shown to impact autophagy [5] and disrupt lysosomal function by increasing Ca^{2+} release and pH [52], potentially contributing to the accumulation of pS65-Ub-labeled mitochondria. While the dynamics of mitophagy are difficult to approximate in post-mortem tissue, both mitochondrial and lysosomal dysfunctions contribute to elevated pS65-Ub levels in cultured cells [57].

Although we observed a strong increase in the density of pS65-Ub containing cells in affected hippocampal subregions in the *MAPT* P301L carrying FTDP-17 brains, there were notable differences both in number and in morphology of pS65-Ub positive structures. In

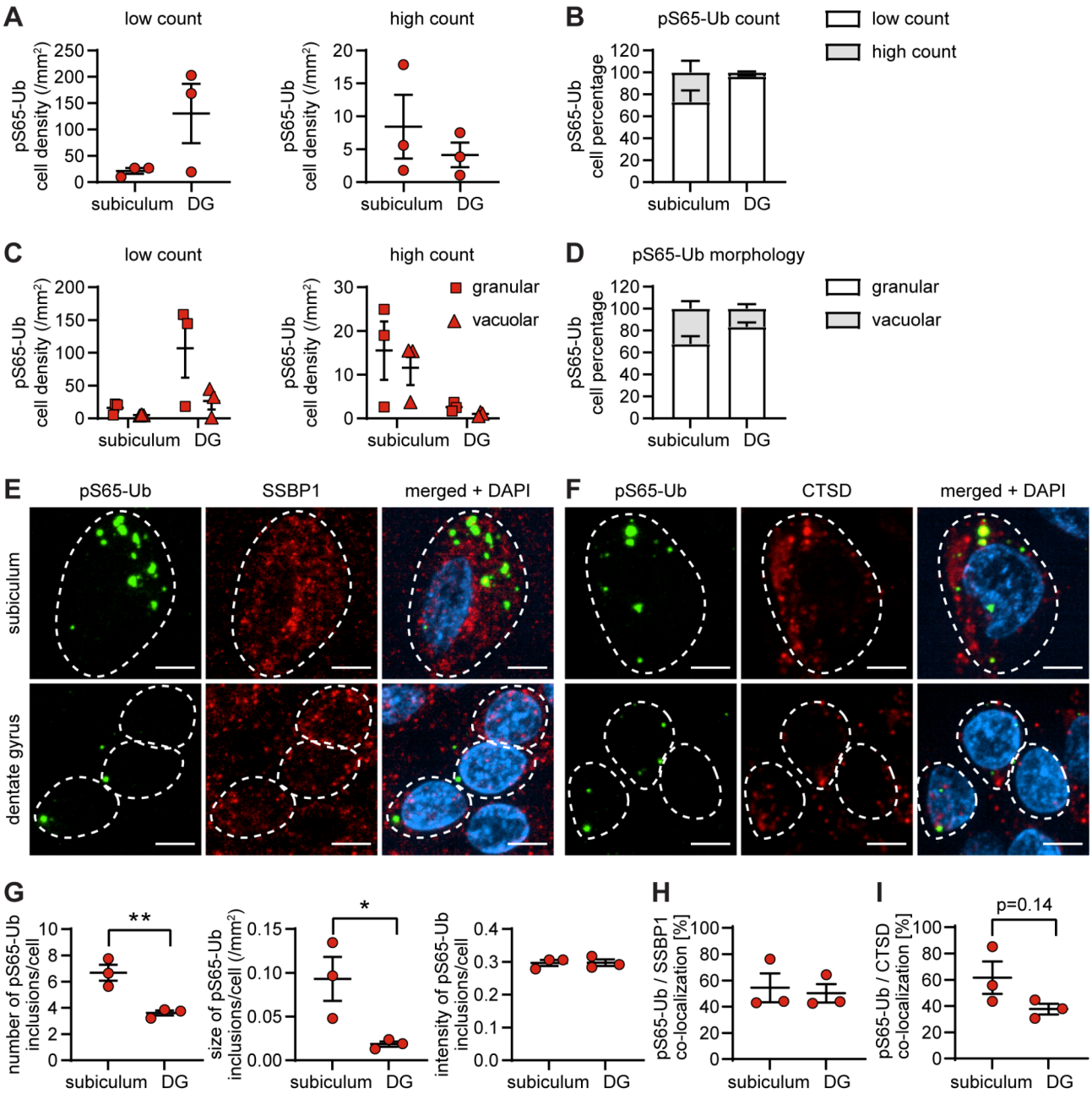

Fig. 5 Increased pS65-Ub localization in lysosomes of the subiculum in FTDP-17 *MAPT* P301L mutant cases. (**A**) Comparison of pS65-Ub cell density between the subiculum and dentate gyrus in low count- and high count-level groups in *MAPT* P301L cases. (**B**) Comparison of pS65-Ub cell percentages between subiculum and dentate gyrus. (**C**) Comparison of the granular and vacuolar pS65-Ub cell densities between the subiculum and dentate gyrus in low- and high-count pS65-Ub cells within *MAPT* P301L cases. (**D**) Comparison of the percentage of granular and vacuolar pS65-Ub cells between the subiculum and dentate gyrus. Higher percentage of vacuolar pS65-Ub cells were found in the subiculum compared to the dentate gyrus. (**E-F**) Representative images of pS65-Ub positive cells co-localized with SSBP1 (E) and CTSD (F) in the subiculum and dentate gyrus. Scale bars: 6.5 µm. Dashed lines represent outline of cells. (**G**) Number, size, and signal intensity of pS65-Ub inclusions per cell in the subiculum compared to the dentate gyrus. (**H-I**) Percentage of pS65-Ub positive puncta that co-localized with SSBP1 (H) or CTSD (I) in the subiculum and dentate gyrus. Data are shown as mean ± SEM. Statistical analysis was performed using unpaired t-test. P301L: $n = 3$. Approximately 30 pS65-Ub positive cells from the subiculum and 60 cells from the dentate gyrus were randomly selected for the analysis. DG = dentate gyrus

the dentate gyrus, pS65-Ub preferentially labeled smaller, granular puncta that were very abundant. In contrast, in the subiculum pS65-Ub predominantly labeled larger, vacuolar structures that were overall less frequent. However, both regions showed a similar high percentage of pS65-Ub deposits that co-localized with a mitochondrial matrix marker. Nevertheless, the larger pS65-Ub positive structures that were found mainly in the subiculum showed greater co-localization also with a lysosomal marker, consistent with their vacuolar appearance. The causes of these notable distinctions are unclear and could be attributed to the differences in mitochondrial network [18], autophagic flux [4], or other intrinsic cellular properties [1] between pyramidal and granule cells. Our study further suggests that mitophagy alterations vary by subregion and may stem from enhanced mitochondrial stress or reduced lysosomal clearance, which could impact certain hippocampal circuitries and associated cognitive function.

The efficient clearance of damaged mitochondria through mitophagy is essential for maintaining mitochondrial homeostasis, cellular bioenergetics, Ca^{2+} signaling, and overall neuronal health (as reviewed in [7, 11, 38]). Conversely, impaired mitophagy leads to the accumulation of dysfunctional mitochondria, disrupting cellular functions and contributing to neurodegeneration [7, 11, 38]. In our study, cells in the subiculum and dentate gyrus, especially the subicular neurons with greater accumulation of damaged mitochondria (as indicated by the number of pS65-Ub inclusions per cell), might be more susceptible to neuronal dysfunction and death compared to cells in other hippocampal subregions such as CA4. However, future research is needed to directly assess hippocampal neuronal (dys-)function and cell loss in FTDP-17 *MAPT* brains and to establish a causal and mechanistic link between mitophagy dysfunctions and selective vulnerability in this disorder.

The current study demonstrated mutant tau-associated alterations in PINK1-PRKN-directed mitophagy in human autopsy brains, but is limited by the availability of tissue samples from this rare autosomal dominant disorder, particularly for the *MAPT* P301L mutation cases. Our findings provide a snapshot of PINK1-PRKN-directed mitophagy alterations at the end-stage of the disease. To gain a more comprehensive understanding of the impact of P301L mutant tau on the dynamic mitophagy process, real-time analyses in cells or in vivo models are needed to monitor the morphology, function, and health of involved organelles, as well as to assess flux of general [36] or selective autophagy [39, 50] over the course of disease progression. Our study only used one phospho-specific tau antibody to assess tau pathology. Additional analyses with other tau antibodies in the future will be helpful to dissect the contribution of distinct tau species and tangle maturation stages to mitophagy alterations. Recent evidence suggests that mitophagy enhancers can reverse P301L tau-induced mitochondrial dysfunction, restoring mitochondrial dynamics, synaptic and mitophagy gene expression, cell survival, and mitochondrial respiration in mouse primary hippocampal neurons [35]. A detailed investigation of mitophagy failure in other brain regions affected in *MAPT*-associated FTDP-17, across different stages of disease, will be critical for guiding future therapeutic strategies.

Conclusions

The current study revealed the diverse mitophagy alteration associated with *MAPT* P301L and N279K mutations in the hippocampus of FTDP-17 brains. We demonstrated significant accumulation of the mitophagy tag pS65-Ub, particularly in regions affected by tau pretangles in the P301L mutation carriers. The differential distribution and morphology of pS65-Ub inclusions across hippocampal subregions suggested that varying degrees of mitochondrial dysfunction and autophagic-lysosomal impairment may underlie the distinct mitophagy alteration observed in these regions. Collectively, our study underscored the relevance of PINK1-PRKN-directed mitophagy in diseases driven by pathogenic tau mutations. These findings provided insights for the exploration of therapeutic strategies mitigating mitochondrial dysfunction in tau-related neurodegenerative diseases.

Abbreviations

4 repeat	4R
AD	Alzheimer's disease
CA	Cornu Ammonis
FTDP-17	frontotemporal dementia with parkinsonism linked to chromosome 17
LBD	Lewy body disease
pS65-Ub	phospho-serine 65 ubiquitin
Ub	ubiquitin

Supplementary Information

The online version contains supplementary material available at https://doi.org/10.1186/s40478-025-01955-8.

Supplementary Material 1

Acknowledgements

We are grateful to the patients and their families who made this study possible. We thank the Neuropathology and Microscopy Laboratory at Mayo Clinic Florida for processing human post-mortem tissues and the excellent technical support. We thank Ms. Audrey Strongosky for her invaluable assistance in logistics of brain specimen procurements. We also thank the late Dr. Peter Davies from the Feinstein Institute for his generous contribution of CP13 antibodies.

Author contributions

Conceptualization: W.S., X.H. Investigation: T.R., X.H. Data Analysis: T.R., X.H., F.C.F. Resources: D.W.D., Z.K.W. Writing: T.R., X.H., W.S., F.C.F. Funding Acquisition: W.S., Z.K.W.

Funding
W.S., F.C.F., D.W.D., and Z.K.W. are members of the American Parkinson Disease Association (APDA) Center for Advanced Research at Mayo Clinic Florida. W.S. and D.W.D. are further supported by the National Institute of Neurological Disorders and Stroke (NIH/NINDS) Lewy Body Dementia Center Without Walls (U54 NS110435). Work in the authors labs is additionally funded by the National Institutes of Health (R56 AG062556, RF1 NS085070, and R01 NS110085 to W.S.), the Department of Defense Congressionally Directed Medical Research Programs (CDMRP) (W81XWH-17-1-0248 to W.S.), the Florida Department of Health - Ed and Ethel Moore Alzheimer's Disease Research Program (9AZ10 to W.S. and 22A07 to F.C.F.), The Ted Nash Long Life Foundation (W.S.) and The Michael J. Fox Foundation for Parkinson's Research (W.S. and F.C.F.). W.S. is also supported by Mayo Clinic Foundation, Mayo Clinic Center for Biomedical Discovery (CBD), and Mayo Clinic Robert and Arlene Kogod Center on Aging. F.C.F is supported by the Mayo Clinic CBD and the Mayo Clinic Office of Research Equity, Inclusion and Diversity. X.H. is supported by a pilot grant and a developmental project award from the Mayo Clinic Alzheimer Disease Research Center (ADRC, P30 AG062677), fellowships awarded by the APDA and Alzheimer's Association (AARF-22-973152), and a pilot grant from the Mayo Clinic CBD. Z.K.W. is partially supported by the National Institute of Aging (U19 AG063911), the Haworth Family Professorship in Neurodegenerative Diseases fund, The Albertson Parkinson's Research Foundation, PPND Family Foundation, and Margaret N. and John Wilchek Family.

Data availability
Access to the datasets used and/or analyzed during the current study are available from the corresponding author Dr. Wolfdieter Springer (Springer.Wolfdieter@mayo.edu) and Dr. Xu Hou (Hou.Xu@mayo.edu) on request.

Declarations

Ethics approval
All brain samples are from autopsies performed after approval by the legal next-of-kin. Research on de-identified postmortem brain tissue is considered exempt from human subjects' regulations by the Mayo Clinic Institutional Review Board.

Consent for publication
Not applicable.

Competing interests
Mayo Clinic, F.C.F., and W.S. hold a patent related to PRKN activators (Small Molecule Activators of Parkin Enzyme Function, US patent, 11401255B2; August 02, 2022). Z.K.W. serves as PI or Co-PI on projects/grants from Biohaven Pharmaceuticals, Inc., Vigil Neuroscience, Inc., ONO Pharmaceuticals Co., LTD., and Amylyx Pharmaceuticals, Inc., and he is an external advisory board member for Vigil Neuroscience, Inc., and a consultant on neurodegenerative medical research for Eli Lilly & Company and NovoGlia Inc. All other authors declare they have no competing interests. This research was conducted in compliance with Mayo Clinic conflict of interest policies.

Received: 22 November 2024 / Accepted: 12 February 2025
Published online: 24 February 2025

References

1. Alkadhi KA (2019) Cellular and Molecular differences between area CA1 and the Dentate Gyrus of the Hippocampus. Mol Neurobiol 56:6566–6580. https://doi.org/10.1007/s12035-019-1541-2
2. Bharat V, Hsieh CH, Wang X (2021) Mitochondrial defects in fibroblasts of pathogenic MAPT patients. Front Cell Dev Biol 9:765408. https://doi.org/10.3389/fcell.2021.765408
3. Boeve BF, Rosen H (2021) Clinical and neuroimaging aspects of Familial Frontotemporal Lobar Degeneration Associated with MAPT and GRN mutations. Adv Exp Med Biol 1281:77–92. https://doi.org/10.1007/978-3-030-51140-1_6
4. Bordi M, Berg MJ, Mohan PS, Peterhoff CM, Alldred MJ, Che S, Ginsberg SD, Nixon RA (2016) Autophagy flux in CA1 neurons of Alzheimer hippocampus: increased induction overburdens failing lysosomes to propel neuritic dystrophy. Autophagy 12:2467–2483. https://doi.org/10.1080/15548627.2016.1239003
5. Caballero B, Wang Y, Diaz A, Tasset I, Juste YR, Stiller B, Mandelkow EM, Mandelkow E, Cuervo AM (2018) Interplay of pathogenic forms of human tau with different autophagic pathways. Aging Cell 17. https://doi.org/10.1111/acel.12692
6. Cabezas-Opazo FA, Vergara-Pulgar K, Perez MJ, Jara C, Osorio-Fuentealba C, Quintanilla RA (2015) Mitochondrial Dysfunction Contributes to the Pathogenesis of Alzheimer's Disease. Oxid Med Cell Longev 2015: 509654 https://doi.org/10.1155/2015/509654
7. Cai Q, Jeong YY (2020) Mitophagy in Alzheimer's Disease and Other Age-Related Neurodegenerative Diseases. Cells 9. https://doi.org/10.3390/cells9010150
8. Clark LN, Poorkaj P, Wszolek Z, Geschwind DH, Nasreddine ZS, Miller B, Li D, Payami H, Awert F, Markopoulou K al (1998) Pathogenic implications of mutations in the tau gene in pallido-ponto-nigral degeneration and related neurodegenerative disorders linked to chromosome 17. Proc Natl Acad Sci U S A 95:13103–13107. https://doi.org/10.1073/pnas.95.22.13103
9. Cummins N, Tweedie A, Zuryn S, Bertran-Gonzalez J, Gotz J (2019) Disease-associated tau impairs mitophagy by inhibiting Parkin translocation to mitochondria. EMBO J 38. https://doi.org/10.15252/embj.201899360
10. David DC, Hauptmann S, Scherping I, Schuessel K, Keil U, Rizzu P, Ravid R, Drose S, Brandt U, Muller WEet al et al (2005) Proteomic and functional analyses reveal a mitochondrial dysfunction in P301L tau transgenic mice. J Biol Chem 280:23802–23814. https://doi.org/10.1074/jbc.M500356200
11. Dawson TM, Dawson VL (2017) Mitochondrial mechanisms of neuronal cell death: potential therapeutics. Annu Rev Pharmacol Toxicol 57:437–454. https://doi.org/10.1146/annurev-pharmtox-010716-105001
12. Delic V, Brownlow M, Joly-Amado A, Zivkovic S, Noble K, Phan TA, Ta Y, Zhang Y, Bell SD, Kurien Cet al et al (2015) Calorie restriction does not restore brain mitochondrial function in P301L tau mice, but it does decrease mitochondrial F0F1-ATPase activity. Mol Cell Neurosci 67:46–54. https://doi.org/10.1016/j.mcn.2015.06.001
13. Delisle MB, Murrell JR, Richardson R, Trofatter JA, Rascol O, Soulages X, Mohr M, Calvas P, Ghetti B (1999) A mutation at codon 279 (N279K) in exon 10 of the tau gene causes a tauopathy with dementia and supranuclear palsy. Acta Neuropathol 98:62–77. https://doi.org/10.1007/s004010051052
14. Dias-Santagata D, Fulga TA, Duttaroy A, Feany MB (2007) Oxidative stress mediates tau-induced neurodegeneration in Drosophila. J Clin Invest 117:236–245. https://doi.org/10.1172/JCI28769
15. Drummond E, Pires G, MacMurray C, Askenazi M, Nayak S, Bourdon M, Safar J, Ueberheide B, Wisniewski T (2020) Phosphorylated tau interactome in the human Alzheimer's disease brain. Brain 143:2803–2817. https://doi.org/10.1093/brain/awaa223
16. Espay AJ, Litvan I (2011) Parkinsonism and frontotemporal dementia: the clinical overlap. J Mol Neurosci 45:343–349. https://doi.org/10.1007/s12031-011-9632-1
17. Fairley LH, Lejri I, Grimm A, Eckert A (2023) Spermidine rescues Bioenergetic and Mitophagy deficits Induced by Disease-Associated Tau Protein. Int J Mol Sci 24. https://doi.org/10.3390/ijms24065297
18. Faitg J, Lacefield C, Davey T, White K, Laws R, Kosmidis S, Reeve AK, Kandel ER, Vincent AE, Picard M (2021) 3D neuronal mitochondrial morphology in axons, dendrites, and somata of the aging mouse hippocampus. Cell Rep 36:109509. https://doi.org/10.1016/j.celrep.2021.109509
19. Fiesel FC, Ando M, Hudec R, Hill AR, Castanedes-Casey M, Caulfield TR, Moussaud-Lamodiere EL, Stankowski JN, Bauer PO, Lorenzo-Betancor Oet al et al (2015) (Patho-)physiological relevance of PINK1-dependent ubiquitin phosphorylation. EMBO Rep 16:1114–1130. https://doi.org/10.15252/embr.201540514
20. Ghetti B, Oblak AL, Boeve BF, Johnson KA, Dickerson BC, Goedert M (2015) Invited review: Frontotemporal dementia caused by microtubule-associated protein tau gene (MAPT) mutations: a chameleon for neuropathology and neuroimaging. Neuropathol Appl Neurobiol 41:24–46. https://doi.org/10.1111/nan.12213
21. Gibson GE, Shi Q (2010) A mitocentric view of Alzheimer's disease suggests multi-faceted treatments. J Alzheimers Dis 20(Suppl 2):S591–607. https://doi.org/10.3233/JAD-2010-100336
22. Goedert M, Spillantini MG (2000) Tau mutations in frontotemporal dementia FTDP-17 and their relevance for Alzheimer's disease. Biochim Biophys Acta 1502:110–121 Doi 10.1016/s0925-4439(00)00037– 5
23. Grimm A, Biliouris EE, Lang UE, Gotz J, Mensah-Nyagan AG, Eckert A (2016) Sex hormone-related neurosteroids differentially rescue bioenergetic deficits

induced by amyloid-beta or hyperphosphorylated tau protein. Cell Mol Life Sci 73:201–215. https://doi.org/10.1007/s00018-015-1988-x
24. Haussmann R, Wysocki M, Brandt MD, Hermann A, Donix M (2017) MAPT mutation associated with frontotemporal dementia and parkinsonism (FTDP-17). Int Psychogeriatr 29:869–871. https://doi.org/10.1017/S1041610216002192
25. Hong M, Zhukareva V, Vogelsberg-Ragaglia V, Wszolek Z, Reed L, Miller BI, Geschwind DH, Bird TD, McKeel D Goate A (1998) mutation-specific functional impairments in distinct tau isoforms of hereditary FTDP-17. Science 282: 1914–1917 https://doi.org/10.1126/science.282.5395.1914
26. Hou X, Fiesel FC, Truban D, Castanedes Casey M, Lin WL, Soto AI, Tacik P, Rousseau LG, Diehl NN, Heckman MG al (2018) Age- and disease-dependent increase of the mitophagy marker phospho-ubiquitin in normal aging and Lewy body disease. Autophagy 14:1404–1418. https://doi.org/10.1080/15548627.2018.1461294
27. Hou X, Watzlawik JO, Cook C, Liu CC, Kang SS, Lin WL, DeTure M, Heckman MG, Diehl NN, Al-Shaikh FSH al (2020) Mitophagy alterations in Alzheimer's disease are associated with granulovacuolar degeneration and early tau pathology. Alzheimers Dement 17:417–430. https://doi.org/10.1002/alz.12198
28. Hou X, Watzlawik JO, Fiesel FC, Springer W (2020) Autophagy in Parkinson's Disease. J Mol Biol 432:2651–2672. https://doi.org/10.1016/j.jmb.2020.01.037
29. Hu Y, Li XC, Wang ZH, Luo Y, Zhang X, Liu XP, Feng Q, Wang Q, Yue Z, Chen Z et al (2016) Tau accumulation impairs mitophagy via increasing mitochondrial membrane potential and reducing mitochondrial Parkin. Oncotarget 7: 17356–17368 https://doi.org/10.18632/oncotarget.7861
30. Iovino M, Agathou S, Gonzalez-Rueda A, Del Castillo Velasco-Herrera M, Borroni B, Alberici A, Lynch T, O'Dowd S, Geti I, Gaffney Det al et al (2015) Early maturation and distinct tau pathology in induced pluripotent stem cell-derived neurons from patients with MAPT mutations. Brain 138:3345–3359. https://doi.org/10.1093/brain/awv222
31. Kandimalla R, Manczak M, Pradeepkiran JA, Morton H, Reddy PH (2022) A partial reduction of Drp1 improves cognitive behavior and enhances mitophagy, autophagy and dendritic spines in a transgenic tau mouse model of Alzheimer disease. Hum Mol Genet 31:1788–1805. https://doi.org/10.1093/hmg/ddab360
32. Khandelwal PJ, Herman AM, Hoe HS, Rebeck GW, Moussa CE (2011) Parkin mediates beclin-dependent autophagic clearance of defective mitochondria and ubiquitinated abeta in AD models. Hum Mol Genet 20:2091–2102. https://doi.org/10.1093/hmg/ddr091
33. Kopeikina KJ, Carlson GA, Pitstick R, Ludvigson AE, Peters A, Luebke JI, Koffie RM, Frosch MP, Hyman BT, Spires-Jones TL (2011) Tau accumulation causes mitochondrial distribution deficits in neurons in a mouse model of tauopathy and in human Alzheimer's disease brain. Am J Pathol 179:2071–2082. https://doi.org/10.1016/j.ajpath.2011.07.004
34. Korn L, Speicher AM, Schroeter CB, Gola L, Kaehne T, Engler A, Disse P, Fernandez-Orth J, Csatari J, Naumann M al (2023) MAPT genotype-dependent mitochondrial aberration and ROS production trigger dysfunction and death in cortical neurons of patients with hereditary FTLD. Redox Biol 59:102597. https://doi.org/10.1016/j.redox.2022.102597
35. Kshirsagar S, Sawant N, Morton H, Reddy AP, Reddy PH (2021) Mitophagy enhancers against phosphorylated tau-induced mitochondrial and synaptic toxicities in Alzheimer disease. Pharmacol Res 174:105973. https://doi.org/10.1016/j.phrs.2021.105973
36. Lee JH, Rao MV, Yang DS, Stavrides P, Im E, Pensalfini A, Huo C, Sarkar P, Yoshimori T, Nixon RA (2019) Transgenic expression of a ratiometric autophagy probe specifically in neurons enables the interrogation of brain autophagy in vivo. Autophagy 15:543–557. https://doi.org/10.1080/15548627.2018.1528812
37. Liu C, Song X, Nisbet R, Gotz J (2016) Co-immunoprecipitation with tau isoform-specific antibodies reveals distinct protein interactions and highlights a putative role for 2 N tau in Disease. J Biol Chem 291:8173–8188. https://doi.org/10.1074/jbc.M115.641902
38. Lou G, Palikaras K, Lautrup S, Scheibye-Knudsen M, Tavernarakis N, Fang EF (2020) Mitophagy and Neuroprotection. Trends Mol Med 26:8–20. https://doi.org/10.1016/j.molmed.2019.07.002
39. McWilliams TG, Prescott AR, Allen GF, Tamjar J, Munson MJ, Thomson C, Muqit MM, Ganley IG (2016) mito-QC illuminates mitophagy and mitochondrial architecture in vivo. J Cell Biol 214:333–345. https://doi.org/10.1083/jcb.201603039
40. Miyasaka T, Morishima-Kawashima M, Ravid R, Kamphorst W, Nagashima K, Ihara Y (2001) Selective deposition of mutant tau in the FTDP-17 brain affected by the P301L mutation. J Neuropathol Exp Neurol 60:872–884. https://doi.org/10.1093/jnen/60.9.872
41. Moloney CM, Lowe VJ, Murray ME (2021) Visualization of neurofibrillary tangle maturity in Alzheimer's disease: a clinicopathologic perspective for biomarker research. Alzheimers Dement 17:1554–1574. https://doi.org/10.1002/alz.12321
42. Moloney CM, Labuzan SA, Crook JE, Siddiqui H, Castanedes-Casey M, Lachner C, Petersen RC, Duara R, Graff-Radford NR Dickson DW (2022) Phosphorylated tau sites that are elevated in Alzheimer's disease fluid biomarkers are visualized in early neurofibrillary tangle maturity levels in the post mortem brain. Alzheimers Dement: Doi https://doi.org/10.1002/alz.12749
43. Olszewska DA, Lonergan R, Fallon EM, Lynch T (2016) Genetics of Frontotemporal Dementia. Curr Neurol Neurosci Rep 16:107. https://doi.org/10.1007/s11910-016-0707-9
44. Reed LA, Wszolek ZK, Hutton M (2001) Phenotypic correlations in FTDP-17. Neurobiol Aging 22:89–107. https://doi.org/10.1016/s0197-4580(00)00202-5
45. Rhein V, Song X, Wiesner A, Ittner LM, Baysang G, Meier F, Ozmen L, Bluethmann H, Drose S, Brandt Uet al et al (2009) Amyloid-beta and tau synergistically impair the oxidative phosphorylation system in triple transgenic Alzheimer's disease mice. Proc Natl Acad Sci U S A 106:20057–20062. https://doi.org/10.1073/pnas.0905529106
46. Rodriguez-Martin T, Pooler AM, Lau DHW, Morotz GM, De Vos KJ, Gilley J, Coleman MP, Hanger DP (2016) Reduced number of axonal mitochondria and tau hypophosphorylation in mouse P301L tau knockin neurons. Neurobiol Dis 85:1–10. https://doi.org/10.1016/j.nbd.2015.10.007
47. Schulz KL, Eckert A, Rhein V, Mai S, Haase W, Reichert AS, Jendrach M, Muller WE, Leuner K (2012) A new link to mitochondrial impairment in tauopathies. Mol Neurobiol 46:205–216. https://doi.org/10.1007/s12035-012-8308-3
48. Spillantini MG, Bird TD, Ghetti B (1998) Frontotemporal dementia and parkinsonism linked to chromosome 17: a new group of tauopathies. Brain Pathol 8:387–402. https://doi.org/10.1111/j.1750-3639.1998.tb00162.x
49. Strang KH, Golde TE, Giasson BI (2019) MAPT mutations, tauopathy, and mechanisms of neurodegeneration. Lab Invest 99:912–928. https://doi.org/10.1038/s41374-019-0197-x
50. Sun N, Yun J, Liu J, Malide D, Liu C, Rovira II, Holmstrom KM, Fergusson MM, Yoo YH, Combs CAet al et al (2015) Measuring in Vivo Mitophagy. Mol Cell 60:685–696. https://doi.org/10.1016/j.molcel.2015.10.009
51. Tacik P, Sanchez-Contreras M, DeTure M, Murray ME, Rademakers R, Ross OA, Wszolek ZK, Parisi JE, Knopman DS, Petersen RC al (2017) Clinicopathologic heterogeneity in frontotemporal dementia and parkinsonism linked to chromosome 17 (FTDP-17) due to microtubule-associated protein tau (MAPT) p.P301L mutation, including a patient with globular glial tauopathy. Neuropathol Appl Neurobiol 43:200–214. https://doi.org/10.1111/nan.12367
52. Tong BC, Huang AS, Wu AJ, Iyaswamy A, Ho OK, Kong AH, Sreenivasmurthy SG, Zhu Z, Su C, Liu J al (2022) Tetrandrine ameliorates cognitive deficits and mitigates tau aggregation in cell and animal models of tauopathies. J Biomed Sci 29:85. https://doi.org/10.1186/s12929-022-00871-6
53. Tracy TE, Madero-Perez J, Swaney DL, Chang TS, Moritz M, Konrad C, Ward ME, Stevenson E, Huttenhain R Kauwe G (2022) Tau interactome maps synaptic and mitochondrial processes associated with neurodegeneration. Cell 185: 712–728 e714 https://doi.org/10.1016/j.cell.2021.12.041
54. Truban D, Hou X, Caulfield TR, Fiesel FC, Springer W (2017) PINK1, Parkin, and mitochondrial Quality Control: what can we learn about Parkinson's Disease Pathobiology? J Parkinsons Dis 7:13–29. https://doi.org/10.3233/JPD-160989
55. Tsuboi Y (2006) Neuropathology of familial tauopathy. Neuropathology 26:471–474. https://doi.org/10.1111/j.1440-1789.2006.00702.x
56. Vijayan M, Alvir RV, Alvir RV, Bunquin LE, Pradeepkiran JA, Reddy PH (2022) A partial reduction of VDAC1 enhances mitophagy, autophagy, synaptic activities in a transgenic tau mouse model. Aging Cell 21:e13663. https://doi.org/10.1111/acel.13663
57. Watzlawik JO, Hou X, Fricova D, Ramnarine C, Barodia SK, Gendron TF, Heckman MG, DeTure M, Siuda J, Wszolek ZK al (2021) Sensitive ELISA-based detection method for the mitophagy marker p-S65-Ub in human cells, autopsy brain, and blood samples. Autophagy 17:2613–2628. https://doi.org/10.1080/15548627.2020.1834712
58. Weitzman SA, Narasimhan S, He Z, Changolkar L, McBride JD, Zhang B, Schellenberg GD, Trojanowski JQ, Lee VMY (2020) Insoluble tau from human FTDP-17 cases exhibit Unique Transmission properties in vivo. J Neuropathol Exp Neurol 79:941–949. https://doi.org/10.1093/jnen/nlaa086
59. Wren MC, Zhao J, Liu CC, Murray ME, Atagi Y, Davis MD, Fu Y, Okano HJ, Ogaki K, Strongosky AJet al et al (2015) Frontotemporal dementia-associated N279K tau mutant disrupts subcellular vesicle trafficking and induces cellular stress

in iPSC-derived neural stem cells. Mol Neurodegener 10:46. https://doi.org/10.1186/s13024-015-0042-7
60. Wszolek ZK, Pfeiffer RF, Bhatt MH, Schelper RL, Cordes M, Snow BJ, Rodnitzky RL, Wolters EC, Arwert F, Calne DB (1992) Rapidly progressive autosomal dominant parkinsonism and dementia with pallido-ponto-nigral degeneration. Ann Neurol 32:312–320. https://doi.org/10.1002/ana.410320303
61. Wszolek ZK, Tsuboi Y, Ghetti B, Pickering-Brown S, Baba Y, Cheshire WP (2006) Frontotemporal dementia and parkinsonism linked to chromosome 17 (FTDP-17). Orphanet J Rare Dis 1:30. https://doi.org/10.1186/1750-1172-1-30
62. Ye X, Sun X, Starovoytov V, Cai Q (2015) Parkin-mediated mitophagy in mutant hAPP neurons and Alzheimer's disease patient brains. Hum Mol Genet 24:2938–2951. https://doi.org/10.1093/hmg/ddv056

Publisher's note